Supporting information for the article:

Introducing Structure-Switching Functionality into Small-Molecule-Binding Aptamers via Nuclease-Directed Truncation

Zongwen Wang,[1,2] Haixiang Yu,[1] Juan Canoura,[1] Yingzhu Liu,[1] Obtin Alkhamis,[1] Fengfu Fu[3] and Yi Xiao[1*]

[1]Department of Chemistry and Biochemistry, Florida International University, 11200 SW 8th Street, Miami, FL, USA, 33199; [2]Department of Plant Protection, Fujian Agriculture and Forestry University, Fuzhou, China, 350002; [3]Ministry of Education Key Laboratory of Analysis and Detection for Food Safety, Fujian Provincial Key Laboratory of Analysis and Detection Technology for Food Safety, Department of Chemistry, Fuzhou University, Fuzhou, China, 350108.

*Corresponding author: yxiao2@fiu.edu

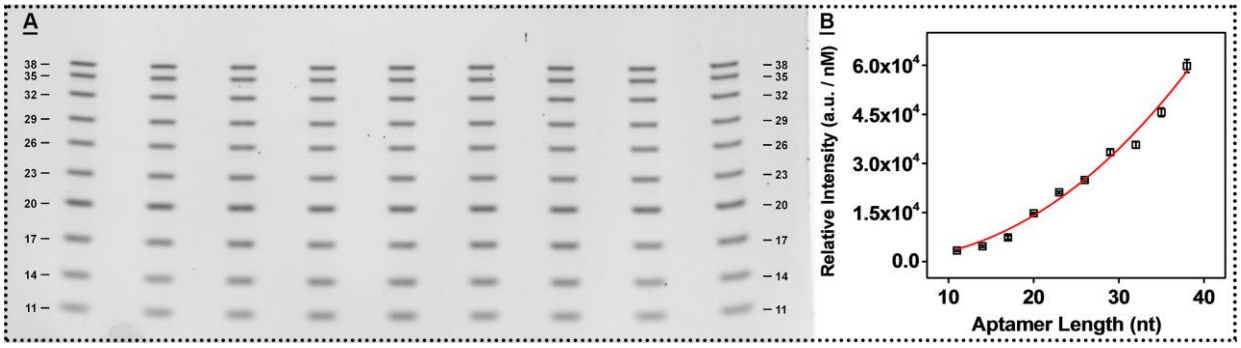

Figure S1. Utilizing a customized DNA ladder to generate a curve for calculating the concentrations of digestion products. (**A**) PAGE analysis of the DNA ladder. Respective concentrations of the 38-, 35-, 32-, 29-, 26-, 23-, 20-, 17-, 14-, and 11-nt in loading buffer are 20, 25, 32, 34, 46, 60, 80, 200, 300 and 400 nM. (**B**) Plot of each band's intensity divided by concentration versus fragment length. Error bars represent standard deviation of nine measures in one gel.

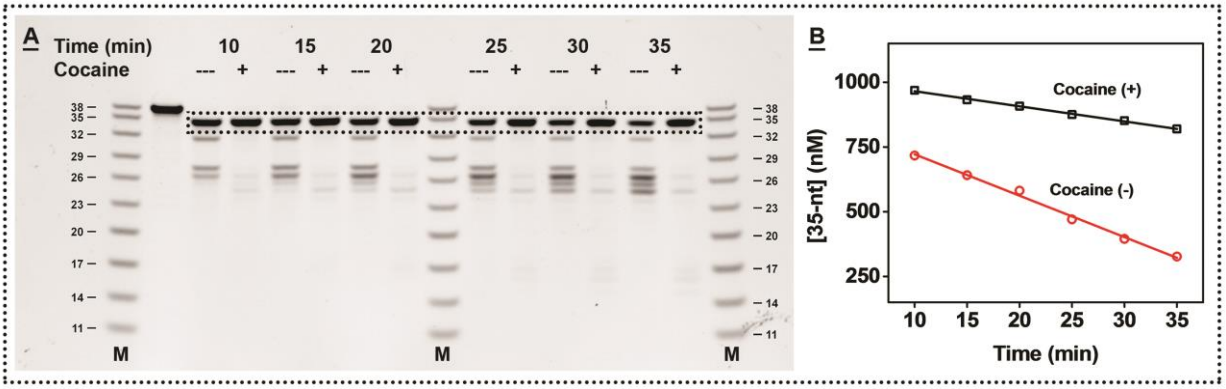

Figure S2. Time course of 38-GC Exo III digestion in the absence or presence of cocaine. (**A**) PAGE analysis of digestion products. (**B**) Extent of 35-nt product degradation over time in the presence or absence of cocaine. [38-GC]: 1 μM, [cocaine]: 250 μM, [Exo III]: 0.26 U/μL.

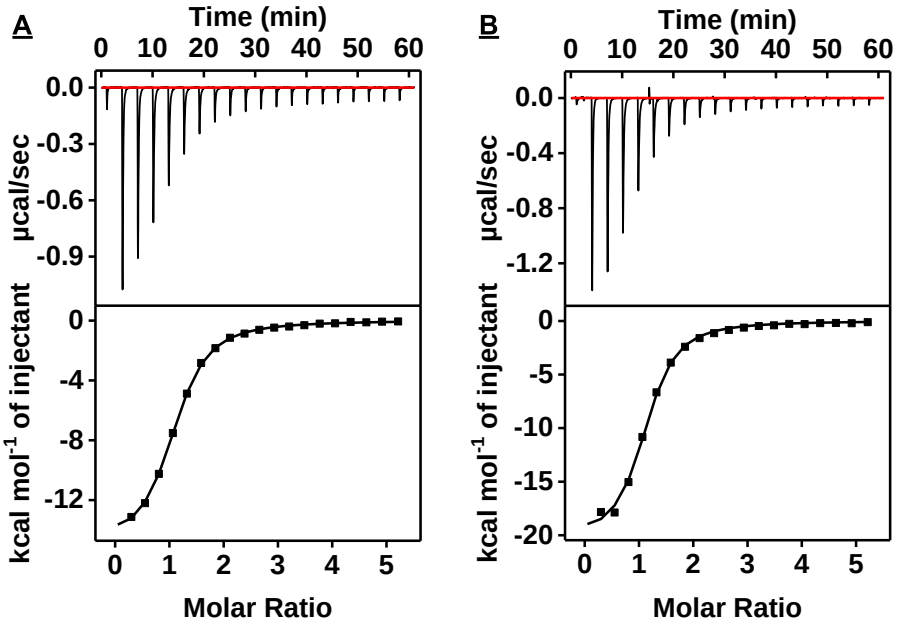

Figure S3. Characterization of target affinity of cocaine-binding aptamers using isothermal titration calorimetry (ITC). Top panels present raw data showing the heat generated from each titration of cocaine for (**A**) 38-GC and (**B**) 38-GT. Bottom panels show the integrated heat of each titration after correcting for dilution heat of the titrant.

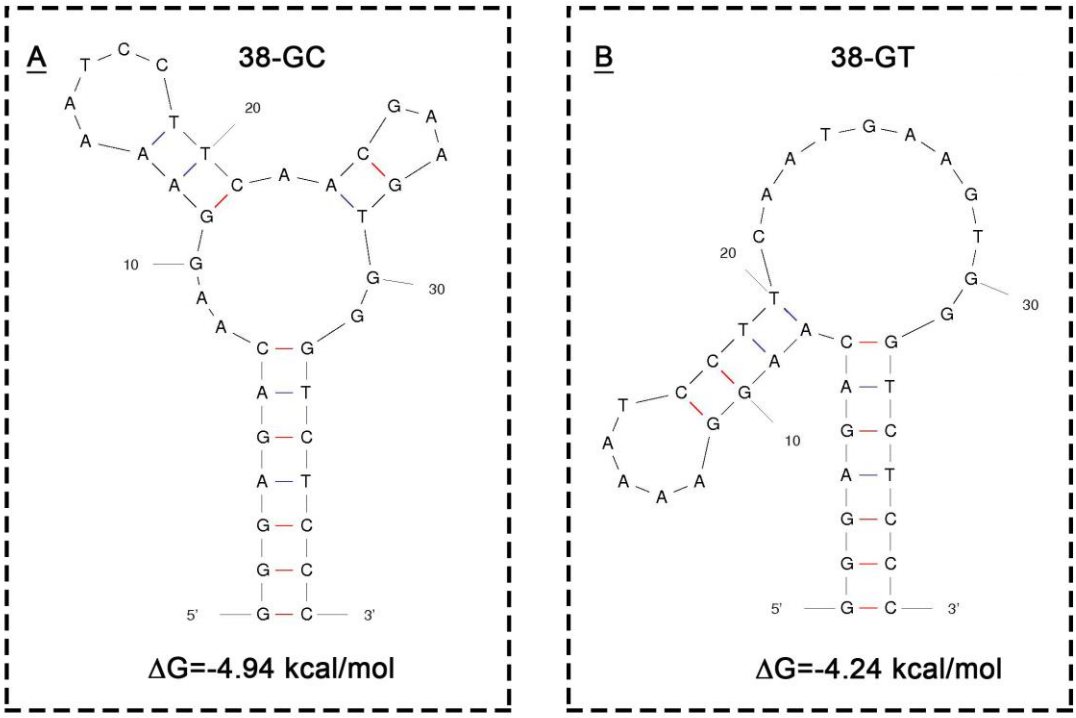

Figure S4. Mfold predicted structures of (**A**) 38-GC and (**B**) 38-GT at 23 °C. Free energy values are listed below each structure.

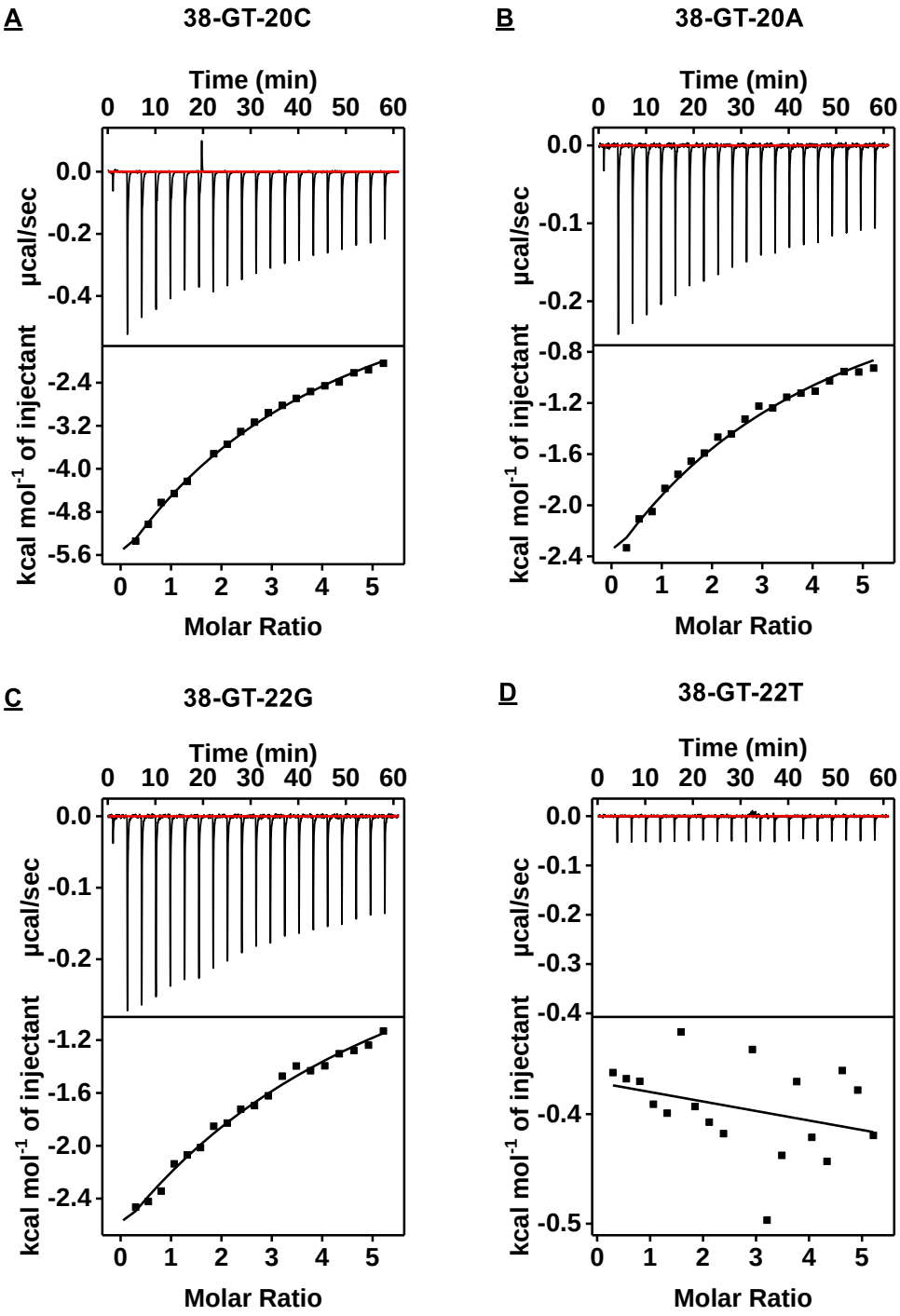

Figure S5. Characterization of cocaine binding affinity of 38-GT mutants using ITC. Top panels present raw data showing the heat generated from each titration of cocaine for (**A**) 38-GT-20C, (**B**) 38-GT-20A, (**C**) 38-GT-22G and (**D**) 38-GT-22T. Bottom panels show the integrated heat of each titration after correcting for dilution heat of the titrant.

Figure S6. Specific Exo III inhibition of cocaine-aptamer complexes. (**A**) PAGE analysis of digestion products of 38-GT and the 38-GT-20C mutant at different cocaine concentrations up to 2 mM. (**B**) A plot of the estimated concentration of the 35-nt product at different concentrations of cocaine after a 25-min reaction. [aptamer]: 1 μM, [Exo III]: 0.26 U/μL.

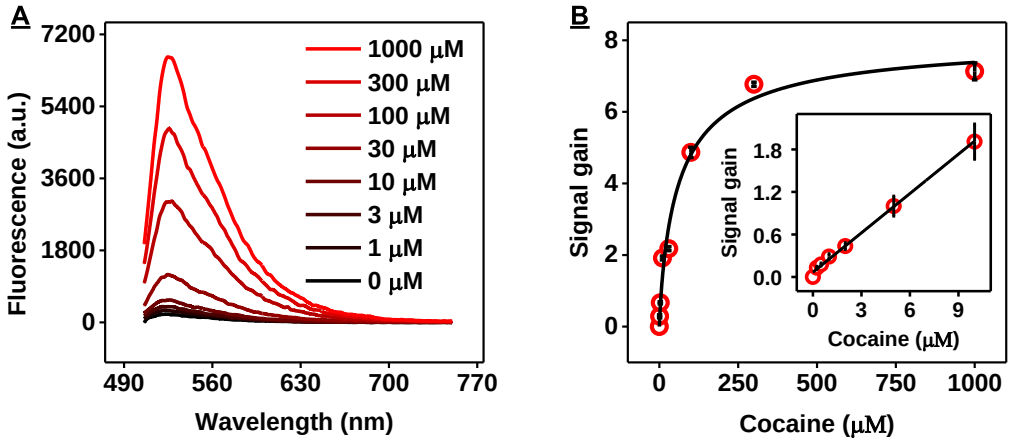

Figure S7. Using our Exo III-based assay to detect cocaine in 10% saliva. (**A**) Fluorescence spectra for Exo III-treated samples with different concentrations of cocaine in 10% saliva. (**B**) Calibration curve with SYBR Green I. Inset depicts the signal gain from 0 to 10 μM. [38-GT]: 1 μM, [Exo III]: 0.26 U/μL.

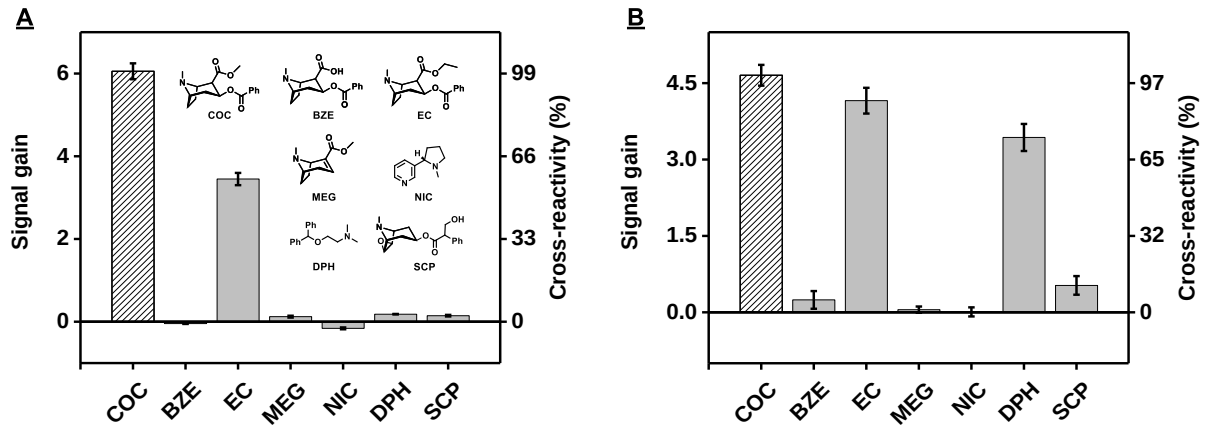

Figure S8. Our Exo III-based fluorescence assay achieves high specificity for cocaine. (**A**) Specificity of Exo III digestion in the presence of cocaine (COC), benzoylecgonine (BZM), cocaethylene (EC), methylecgonidine (MEG), nicotine (NIC), diphenhydramine (DPH), and scopolamine (SCP) in 10% saliva. [target/interferents]: 250 μM, [38-GT]: 1 μM, [Exo III]: 0.26 U/ μl. (**B**) Specificity of detection with 38-GT in an ATMND displacement assay using the same set of drugs. [target/interferents]: 250 μM, [38-GT]: 2 μM, [ATMND]: 0.25 μM.

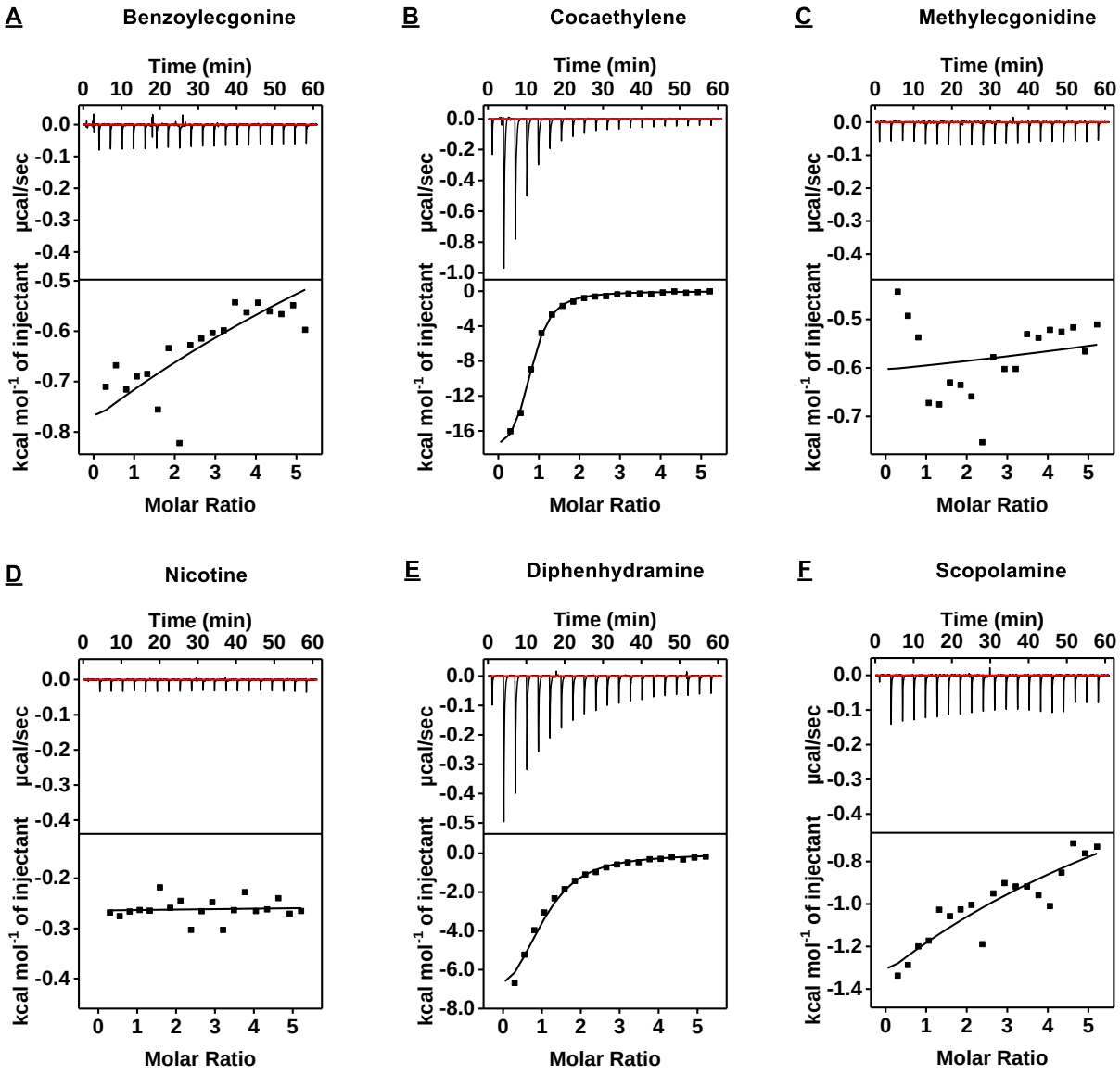

Figure S9. Characterization of binding affinity of 38-GT to interferents using ITC. Top panels present raw data showing the heat generated from each titration of (**A**) benzoylecgonine, (**B**) cocaethylene, (**C**) methylecgonidine, (**D**) nicotine, (**E**) diphenhydramine, and (**F**) scopolamine to 38-GT. Bottom panels show the integrated heat of each titration after correcting for dilution heat of the titrant.

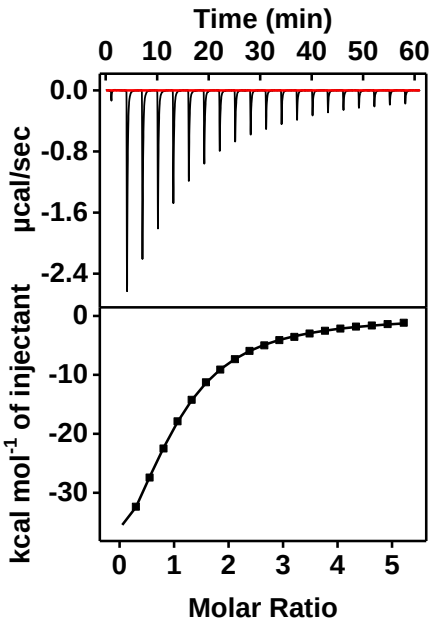

Figure S10. Characterization of binding affinity of 35-GT to cocaine using ITC. Top panels present raw data showing the heat generated from titration of cocaine to 35-GT. Bottom panels show the integrated heat of each titration after correcting for dilution heat of the titrant.

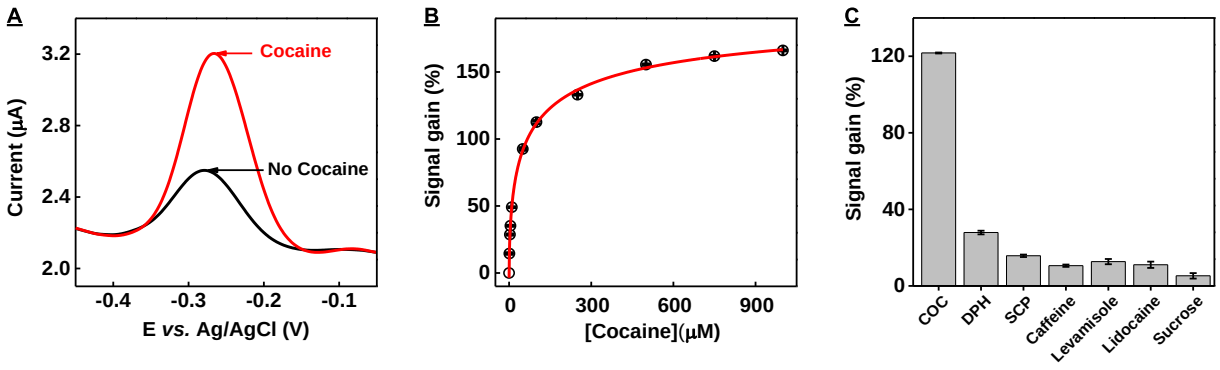

Figure S11. Performance of an E-AB sensor based on the thiolated, methylene blue modified version of Exo III-truncated cocaine-binding aptamer 35-GT. (**A**) Square-wave voltammetry curves of the sensor in the presence and absence of 1,000 µM cocaine. (**B**) Calibration curve of the E-AB sensor for cocaine concentrations ranging from 0-1,000 µM. (**C**) Specificity of the E-AB sensor against cocaine and interferents including diphenhydramine (DPH), scopolamine (SCP), caffeine, levimisole, lidocaine and sucrose.

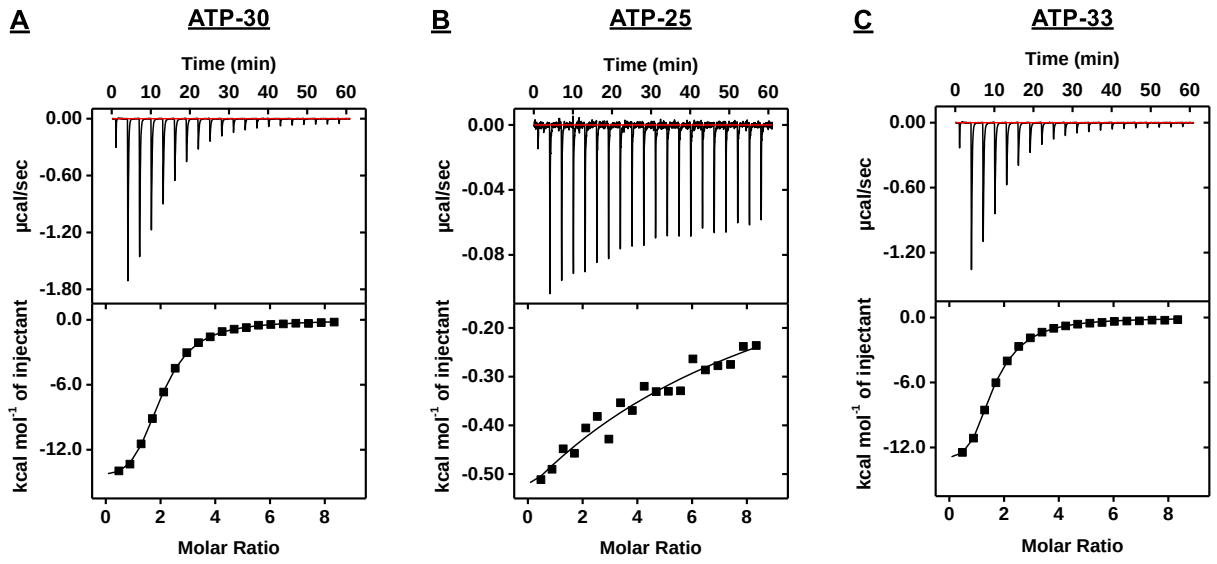

Figure S12. Characterization of target binding affinity of ATP-binding aptamers using ITC. Top panels present raw data showing the heat generated from each titration of ATP for (**A**) ATP-30, (**B**) ATP-25, and (**C**) ATP-33. Bottom panels show the integrated heat of each titration after correcting for dilution heat of the titrant.

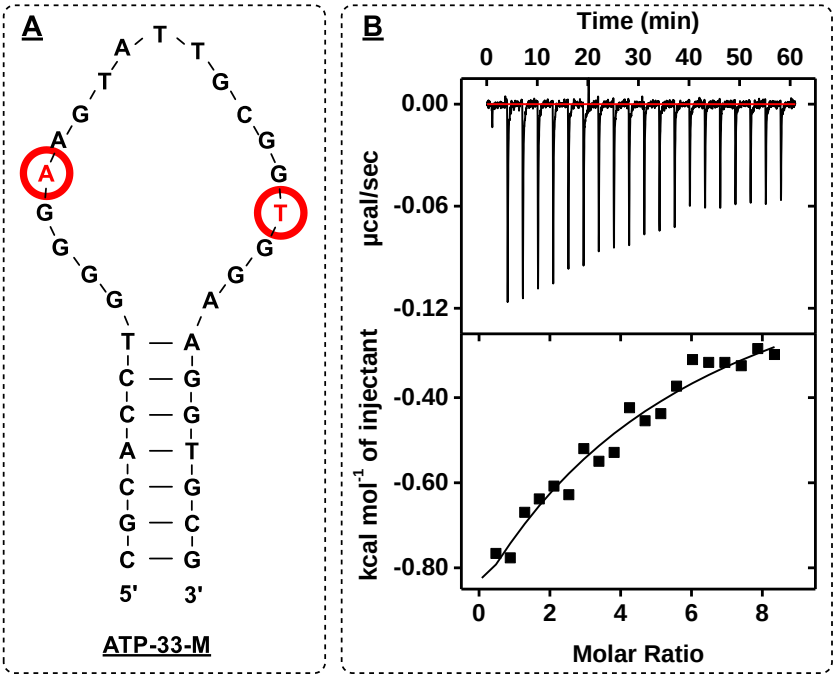

Figure S13. Affinity characterization of ATP-33-M using ITC in 10 mM Tris-HCl, 10 mM $MgCl_2$, pH 7.4, 23 °C. (**A**) Structure of ATP-33-M, with altered nucleotides in red circles. (**B**) Top panels present raw data showing the heat generated from each titration of ATP for ATP-33-M. Bottom panels show the integrated heat of each titration after correcting for dilution heat of the titrant.

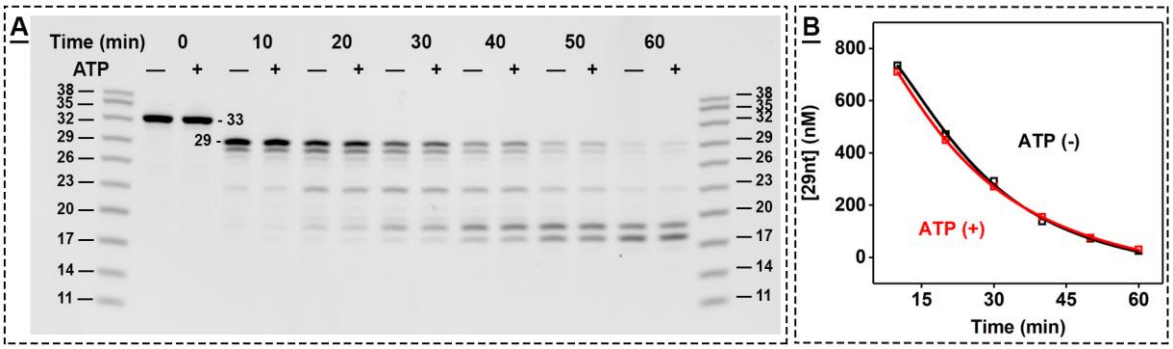

Figure S14. Time course of Exo III digestion for ATP-33-M in the absence or presence of ATP. (**A**) PAGE analysis of Exo III-digestion products over time. (**B**) A plot of the estimated concentration of the 29-nt major product over the course of digestion.

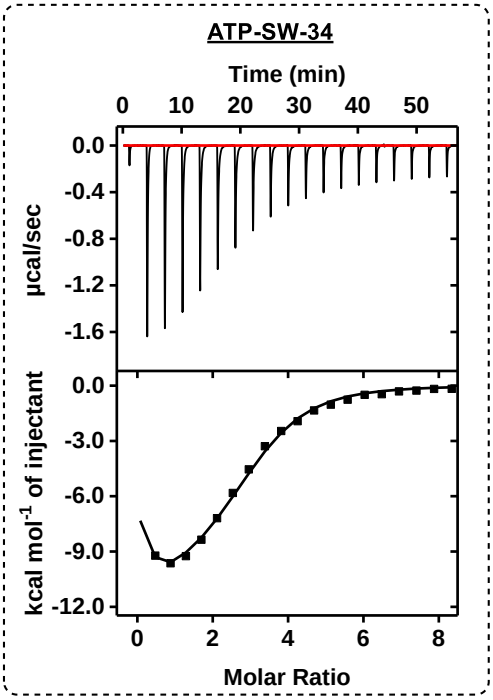

Figure S15. Affinity characterization of structure-switching ATP-binding aptamer under our own experimental conditions (10 mM Tris-HCl, 10 mM $MgCl_2$, pH 7.4, 23 °C) using ITC. Top panels present raw data showing the heat generated from each titration of ATP for ATP-SW-34. Bottom panels show the integrated heat of each titration after correcting for dilution heat of the titrant.

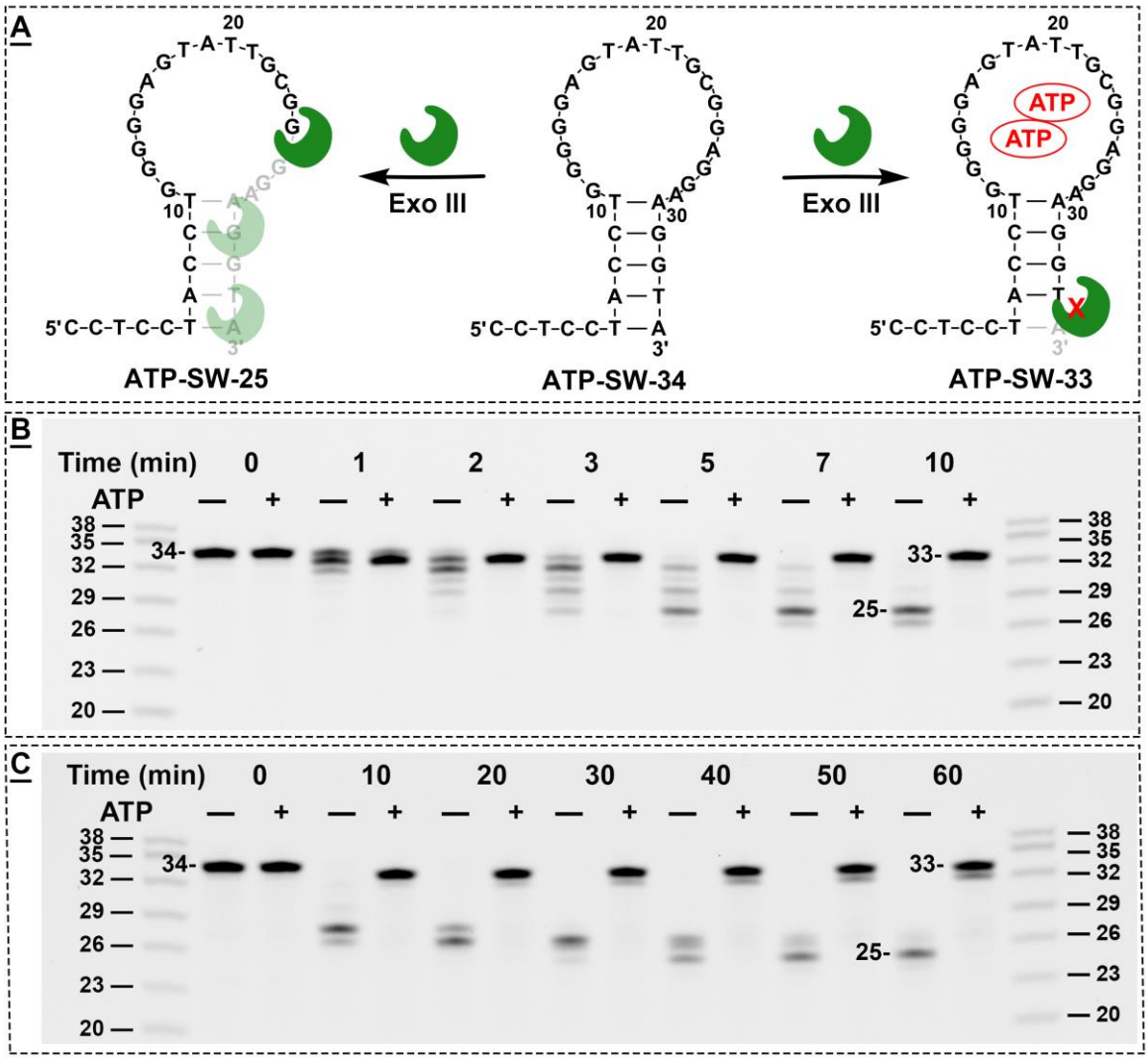

Figure S16. Time course of Exo III digestion for ATP-SW-34 in the absence or presence of ATP under our own experimental conditions (10 mM Tris buffer (pH 7.4) including 10 mM $MgCl_2$, 1 μM DNA, 0.05 U/μL Exo III, 250 μM ATP at 23 °C). (**A**) Schematic of Exo III digestion for ATP-SW-34 with or without target. (**B, C**) PAGE analysis of Exo III-digestion products over (B) 10 and (C) 60 minutes.

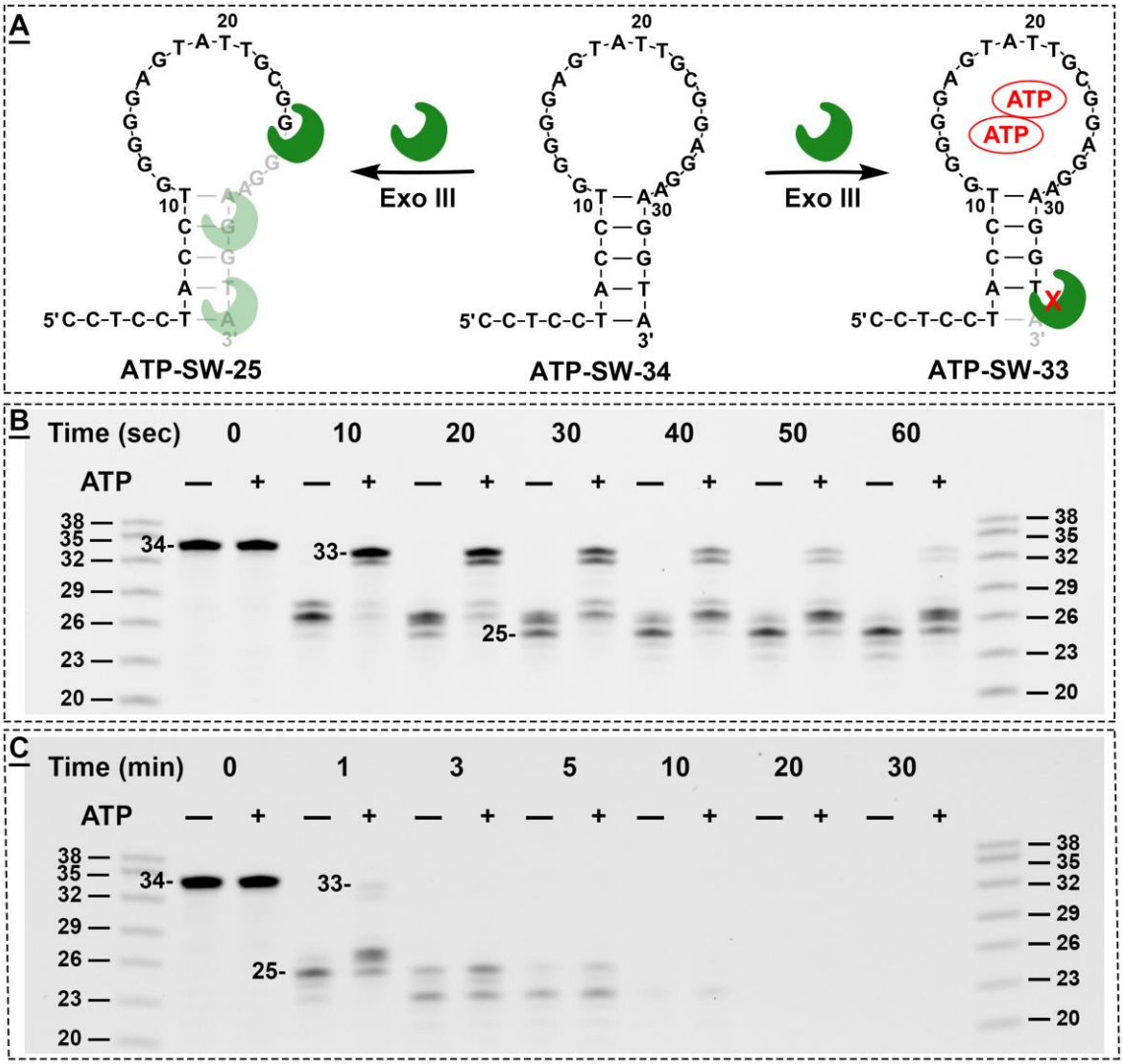

Figure S17. Time course of Exo III digestion for ATP-SW-34 in the absence or presence of ATP under the previously-reported experimental conditions (10 mM Tris buffer (pH 7.9) including 50 mM NaCl, 10 mM $MgCl_2$, 2 μM DNA, 2 U/μL Exo III, 250 μM ATP at 37 °C). (**A**) Schematic of Exo III digestion for ATP-SW-34 with or without target. (**B-C**) PAGE analysis of Exo III-digestion products over (B) 1 minute and (C) 30 minutes.

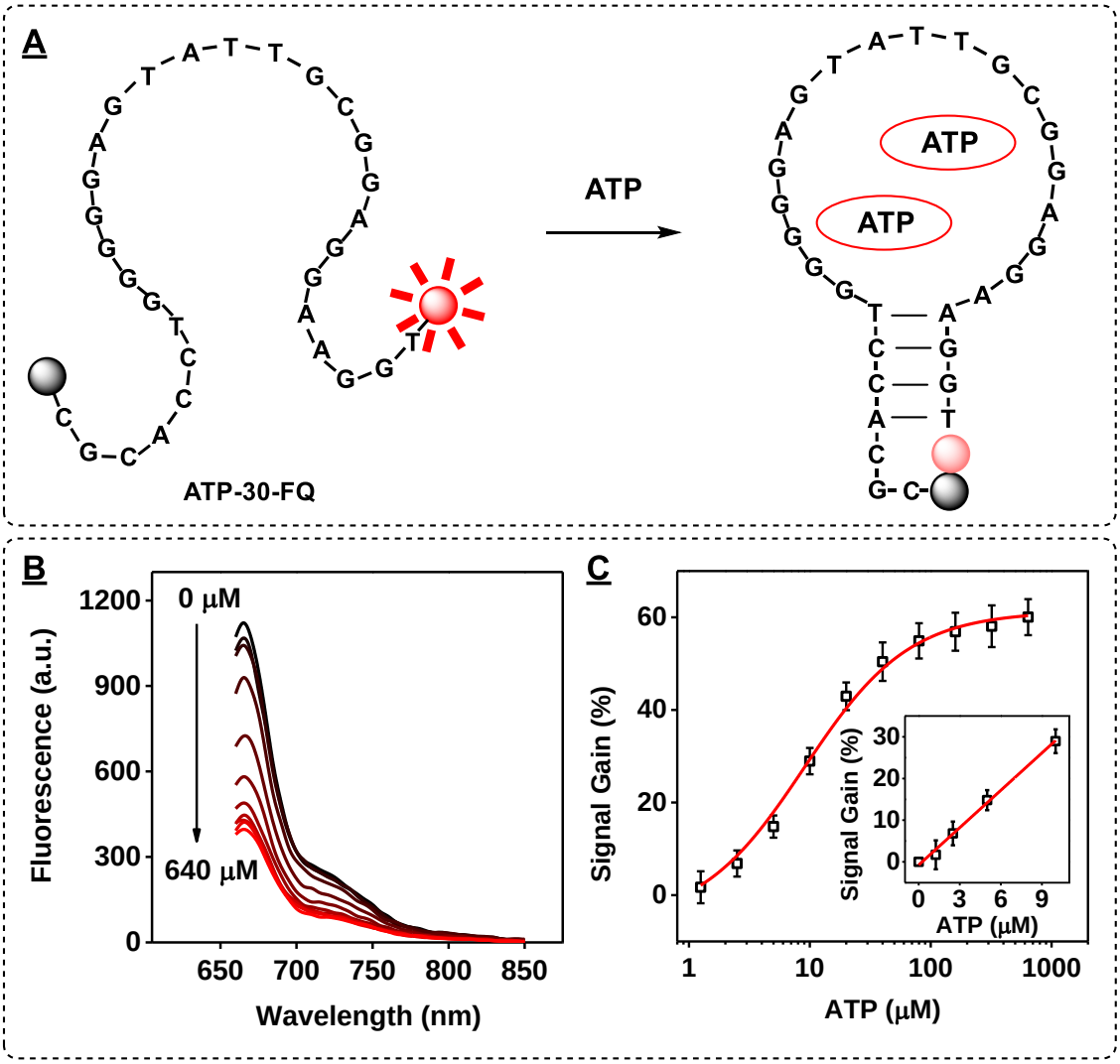

Figure S18. ATP detection with a fluorophore-quencher assay based on the 3' Cy5 fluorophore and a 5' IowaBlack quencher modified version of Exo III-truncated ATP-binding aptamer ATP-30. (**A**) The ATP-30-FQ construct is initially single-stranded, producing strong fluorescence. ATP binding promotes aptamer folding, resulting in quenched fluorescence. (**B**) Fluorescence spectra of ATP detection. From bottom to top, curves depict fluorescence spectra in the presence of 0, 1.25, 2.5, 5, 10, 20, 40, 80, 160, 320, or 640 μM ATP. (**C**) Calibration curve of the assay. Signal gain was calculated using the equation $(F_0 - F)/F_0$ where F and F_0 represent fluorescence intensity at 545 nm in the presence and absence of ATP, respectively. Inset shows the linear range from 0–10 μM ($R^2 = 0.9991$).